

CHANDRA X-RAY DETECTION OF THE RADIO HOTSPOTS OF 3C295

D. E. HARRIS,¹ P. E. J. NULSEN,^{1,2} T. J. PONMAN,^{1,3} M. BAUTZ,⁴ R. A. CAMERON,¹ L. P. DAVID,¹
 R. H. DONNELLY,¹ W. R. FORMAN,¹ L. GREGO,¹ M. J. HARDCASTLE,⁵ J. P. HENRY,⁶ C. JONES,¹
 J. P. LEAHY,⁷ M. MARKEVITCH,¹ A. R. MARTEL,⁸ B. R. MCNAMARA,¹ P. MAZZOTTA,¹ W. TUCKER,¹
 S. N. VIRANI,¹ AND J. VRTILEK¹

submitted to The Astrophysical Journal

ABSTRACT

An observation of the radio galaxy 3C295 during the calibration phase of the Chandra X-ray Observatory reveals X-ray emission from the core of the galaxy, from each of the two prominent radio hotspots, and from the previously known cluster gas. We discuss the possible emission processes for the hotspots and argue that a synchrotron self-Compton model is preferred for most or all of the observed X-ray emission. SSC models with near equipartition fields thus explain the X-ray emission from the hotspots in the two highest surface brightness FR II radio galaxies, Cygnus A and 3C295. This lends weight to the assumption of equipartition and suggests that relativistic protons do not dominate the particle energy density.

Subject headings: galaxies: individual (3C295) – magnetic fields – radiation mechanisms: non-thermal

1. INTRODUCTION

X-ray emission from knots and hotspots in radio jets has been detected in only a handful of objects. The three processes normally considered for X-ray emission from these features are synchrotron, thermal, and synchrotron self-Compton (SSC) emissions. The hotspots of 3C295 (Taylor & Perley 1992) have radio brightness temperatures comparable to those of Cygnus A but are so close to the nucleus that previous X-ray systems could not resolve them. However, the Chandra X-ray Observatory⁹ has the ability not only to separate the emission from the 3C295 cluster gas, core, and hotspots, but in addition, it allows us to obtain spectra of each component.

SSC models predict X-ray intensities in agreement with those observed only for the case of the hotspots of Cygnus A (Harris, Carilli, & Perley 1994). The fact that the observed X-ray flux agrees with the calculated SSC flux for a magnetic field strength equal to the classical estimate from equipartition lends credence to the SSC model but does not prove it. For all the other previously detected knots and hotspots, the predicted SSC flux falls well short of the observed flux, often by two or three orders of magnitude.

In this paper we present Chandra observations of 3C295, describe the basic results, and evaluate the emission process for the X-rays from the radio hotspots. We use $H_0=70 \text{ km s}^{-1} \text{ Mpc}^{-1}$, $\Omega_\Lambda=0.7$, and $\Omega_M=0.3$. At a redshift of 0.461, the luminosity distance is 2564 Mpc and $1''=5.8 \text{ kpc}$. In discussing

power law spectra we follow the convention that the flux density is $S=k\nu^{-\alpha}$.

2. DATA ANALYSIS

The calibration observation of 3C295 was performed on 1999 Aug30 for an elapsed time of 20,408s. The target was near the aim point on the S3 ACIS chip. We generated a clean data set by selecting the standard grade set (0,2,3,4,6), energies less than 10 keV, and excising times with enhanced background rates. The screened exposure time for the observation is 17,792 s.

During standard processing, photon events are assigned fractional pixel locations due to spacecraft dither, rotation between detector and sky coordinates, and an additional randomization within each $0''.5$ ACIS pixel. We used the fractional pixel values to generate images with $0''.1$ pixels. Figure 1 shows the central region after adaptive smoothing with a Gaussian constrained to have $\sigma \geq 0''.3$. Overlaid are the radio contours from a 20 cm MERLIN+VLA image (Leahy et al., in preparation).

2.1. X-ray Morphology

The ACIS-S image in Figure 1 shows that the central region of the 3C295 cluster exhibits significant structure with an X-ray core and two outer features aligned with the radio hotspots. This observation is an excellent example of the resolving power of Chandra. 3C295 was previously observed by the Einstein HRI (Henry & Henriksen 1986) and the ROSAT HRI (Neumann 1999) but the spatial resolution of these instruments was comparable to the separation of the two X-ray hotspots and these features were thus not detected. The ACIS image in Figure 2 shows that the core and two hotspots are not simple, azimuthally symmetric features, suggesting that these regions are resolved by Chandra. To determine if the core and hotspots are extended we must model the cluster emission. The region outside a $3''$ radius is well fit with a β model with $\beta=0.54$ and core radius $a = 4''.1$ (24 kpc). The residual X-ray data above this model are shown superimposed on the HST image in Figure 2. Inside $r = 3''$ there is clearly excess emission above the β model, surrounding the nuclear and hotspot sources. We

¹Harvard-Smithsonian Center for Astrophysics, 60 Garden St. Cambridge, MA 02138

²Department of Engineering Physics, University of Wollongong, Wollongong NSW 2522, Australia

³School of Physics & Astronomy, University of Birmingham, Birmingham B15 2TT, UK

⁴Massachusetts Institute of Technology, Center for Space Research, Cambridge, MA 02139

⁵Dept. Physics, University of Bristol, Tyndall Avenue, Bristol BS8 1TL, UK

⁶Institute for Astronomy, 2680 Woodlawn Drive, Honolulu, HI 96822

⁷University of Manchester, Jodrell Bank Observatory, Macclesfield, Cheshire SK11 9DL, UK

⁸Dept. Physics and Astronomy, Johns Hopkins University 3400 N. Charles Street, Baltimore, MD 21218

⁹<http://asc.harvard.edu/udocs/docs/docs.html>

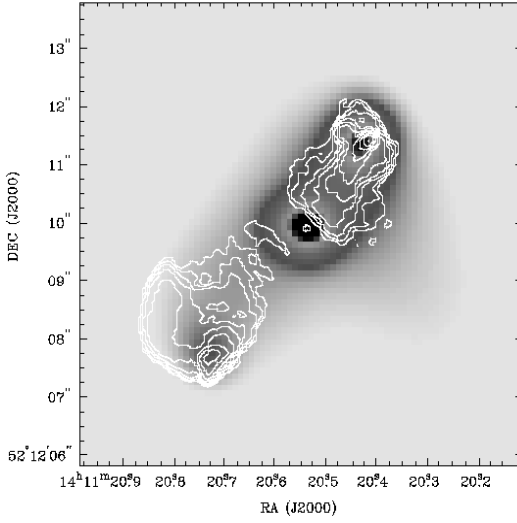


FIG. 1. The 20 cm MERLIN data (contours) overlaid on the ACIS image. The radio contours are logarithmically spaced from 4 mJy to 2.0 Jy, shown with a restoring beamsize of $0''.14$. The X-ray data have been shifted by $0''.66$ to align the X-ray and radio cores. The NW hotspot is at a projected distance of $1''.9$ (11 kpc) from the core and the SE hotspot is $2''.75$ (16 kpc) from the core.

attempted to remove this by fitting a double β model to the data with the nuclear and hotspot regions excluded. This removed the surrounding emission fairly effectively, allowing us to study the size of the central components. To test these components for intrinsic extension, we compared the ratio of net counts in two concentric regions centered on these features in the residual image. The ratios of net counts between 0 and $0''.5$ and from 0.5 to $1''.0$ for the northwest (NW) hotspot, and southeast (SE) hotspot are 1.35 ± 0.38 and 0.97 ± 0.35 , respectively (Poisson errors). We use the ACIS-S image of PKS0637-72 to determine this ratio for an imaged point source, finding a ratio of 1.93 ± 0.08 . Based on this statistic, there is tentative evidence in the Chandra data for some extension of the hot spot X-ray sources. However, this result is subject to uncertainties in the shape of the underlying diffuse distribution. In the case of the nuclear source these systematics are dominant, and no useful extension test is possible.

2.2. X-ray Spectral Results

The response matrices for the S3 chip have been calibrated on 32 by 32 pixel regions. There are also twelve effective area files covering the S3 chip. A separate photon weighted response

TABLE 1
Summary of Spectral Analysis Results

	Cluster	Nucleus	NW	SE
Region	$r=90''$	$r=0''.9$	$1''.5 \times 1''.5$	$r=1''$
Net counts	4856 ± 104	137 ± 15	138 ± 14	42 ± 13
Model	Thermal	PL	PL	...
kT or α	4.4 ± 0.6	-0.8 ± 0.3	0.9 ± 0.5	...
χ^2/DOF	173/143	5.3/4	3.1/3	...
Flux	120.	19.0	3.8	1.1
Lum	9.6×10^{44}	7.3×10^{43}	2.9×10^{43}	9×10^{42}

Notes: The temperatures are given in keV; the confidence ranges for the spectral parameters are for $\Delta\chi^2=2.7$ (90% for one parameter). The fluxes are 'unabsorbed' for the 0.2 to 10 keV band at the Earth in units of 10^{-14} erg cm $^{-2}$ s $^{-1}$. The source's rest frame luminosity in the 0.2 to 10 keV band is given in ergs s $^{-1}$.

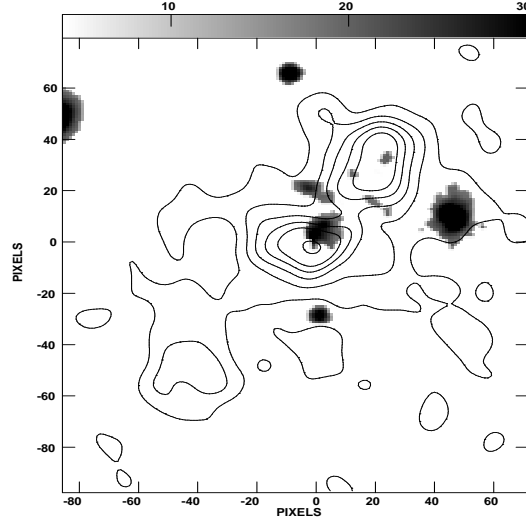


FIG. 2. A contour map of the residual Chandra image after subtraction of the best fit β model superimposed on the residual optical emission from an HST observation after subtracting the emission from the central galaxy. The X-ray data have been smoothed with a Gaussian function of FWHM= $0''.5$. Contour levels are 8, 24, 40, 56, 72, 104 counts per square arcsecond. Coordinate pixels are $0''.045$.

matrix and area file was generated for each extracted spectrum based on the chip coordinates of the detected photons. Spectral bins were chosen to include at least 25 net counts per bin, and the data were fit over the energy range from 0.5 to 7 keV. The results are summarized in Table 1.

2.2.1. The cluster gas

A spectrum was extracted for the whole cluster within $90''$ of the radio nucleus, excluding the central radio source, hotspots, and two background sources. A background spectrum was extracted $\sim 5''.3$ northwest of the cluster center. An absorbed single temperature thermal model, with N_H fixed at 1.34×10^{20} cm $^{-2}$ (the galactic value) provides an adequate fit for abundances from 0.2 to 0.5 cosmic. The results in Table 1 are based on a fixed value of 0.3 for the abundance. Our temperature is not formally consistent with the $7.13^{+2.06}_{-1.35}$ keV obtained from analysis of ASCA data by Mushotzky & Scharf (1997) but our analysis is confined to the central $90''$ and excludes the emission from the core and two hotspots. A more detailed discussion of the cluster emission will be presented in a subsequent paper.

2.2.2. The hotspots

There are insufficient counts to perform a spectral analysis of the SE hotspot. For the NW hotspot, a spectrum was extracted from a $1''.5$ square around the X-ray peak, centered $1''.9$ from the nucleus. There are no counts above 3.5 keV and only 5 bins are used in the fit.

In order to minimize contamination by cluster thermal emission we used a background spectrum extracted from an identical area at a position $1''.8$ SW from the nucleus, in a direction perpendicular to the radio jets. The results for a power law fit are given in Table 1. A thermal model (with $N_H = 1.34 \times 10^{20}$ cm $^{-2}$ and $Z = 0.3$ fixed) gives a best fit temperature of $kT = 4.4^{+19}_{-2.2}$ keV and $\chi^2 = 5.1$ for 3 degrees of freedom, which is also acceptable.

TABLE 2

Uniform Density Hot Gas: Thermal Model Parameters

	Size (arcsec)	Mass (M_{\odot})	n_e (cm^{-3})	P (erg cm^{-3})	RM (rad m^{-2})
NW	$r=0.1$	2.9×10^8	12	1.7×10^{-7}	58,000.
	$r=0.75$	5.9×10^9	0.60	8.2×10^{-9}	21,000.
SE	$r=0.1$	1.6×10^8	6.8	9.2×10^{-8}	32,000.
	$r=0.75$	3.3×10^9	0.33	4.5×10^{-9}	12,000.

Notes: the total mass (Mass), electron number density (n_e), and pressure (P) required to reproduce the observed X-ray emission, assuming a temperature of 4.4 keV. The computed rotation measure (RM) assumes $B=10\mu\text{G}$ and a path length equal to r .

2.2.3. The nucleus

An X-ray spectrum was extracted from a region $0''.9$ in radius around the central peak. In order to remove cluster thermal emission, the background for this spectrum was taken to be the same as that for the northern hotspot. The spectrum is extremely hard; most of the photons have $E > 1\text{keV}$ and about half have $E > 3\text{keV}$.

An absorbed power law fit provides an adequate representation with the best fitting column density consistent with that from galactic foreground absorption. Thermal fits are unacceptable with χ^2 per degree of freedom $> 34/3$. Since the best fit value for α corresponds to a rather steep inverted spectrum, we also attempted fits with column densities up to 10^{24}cm^{-2} , but these all gave a worse fit due to the low energy photons in the spectrum. This could be caused by residual thermal emission, but there are not enough events to pursue this further.

2.3. Other data

MERLIN and VLA data between 1.5 and 43 GHz were taken from Perley & Taylor (1991) and Leahy et al. (in preparation).

We obtained archival HST data and after subtracting the emission from the central galaxy obtained a flux of $S=0.078\mu\text{Jy}$ at $\nu=4.32 \times 10^{14}\text{Hz}$ for the NW hotspot (with a one σ uncertainty of 20%) within a $0''.1$ radius aperture. The optical emission from the hotspot appears to be extended on the same scale as the brightest radio structure and there are fainter features extending back about $0''.5$ towards the galaxy center. The SE hotspot is marginally detected at 3σ with a flux density of $S=0.02\mu\text{Jy}$ (not visible in Figure 2).

3. EMISSION PROCESSES FOR THE HOTSPOTS

3.1. Thermal model for the NW hotspot X-ray emission

We have calculated the electron density required to produce the observed L_x for a temperature of 4.4 keV and two representative volumes: (a) for a sphere with radius $0''.1$ (i.e. the 'unresolved' case) and (b) a sphere with radius $0''.75$ (the maximum size allowed by the data). The resulting values are shown in Table 2, along with the excess rotation measure predicted for a B field component along the line of sight of $10\mu\text{G}$ and a path length equal to the radius of the sphere.

Combining the best fit β model and the X-ray luminosity of 3C295 yields a central electron density of 0.083cm^{-3} . For a temperature of 4.4 keV, this gives an ambient gas pressure of $1.1 \times 10^{-9}\text{erg cm}^{-3}$. The minimum pressure in the NW hotspot is $7 \times 10^{-8}\text{erg cm}^{-3}$ (Taylor & Perley 1992), and hence the jet could drive a shock into the surrounding gas. Applying the

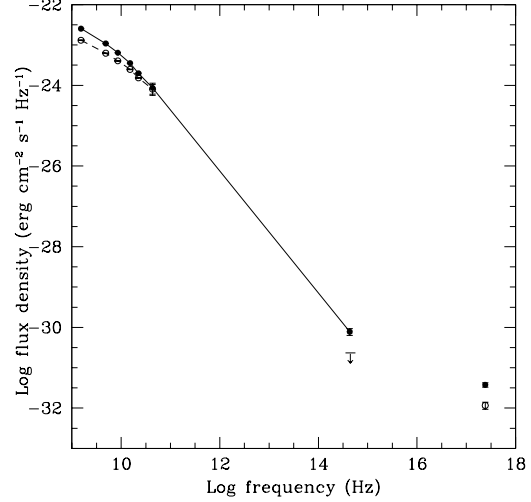


FIG. 3. The observed spectrum of the hotspots. The data for the NW and SE hotspots are shown as filled and open circles, respectively. The 3σ optical flux density for the SE hotspot is shown as an upper-limit. The X-ray data are plotted at 1 keV ($\log \nu = 17.38$).

shock jump conditions for a postshock pressure of $8.2 \times 10^{-9}\text{erg cm}^{-3}$ (the most favorable case from Table 2), gives a postshock density and temperature of 0.22cm^{-3} and 12 keV, respectively. Although this high temperature is allowable within our 90% confidence range, the density is still below the values required to account for the X-ray luminosity (Table 2), and the cooling time of the shocked gas ($\sim 3 \times 10^8\text{yr}$) is far too long for post-shock cooling to allow a rise in density. For a smaller X-ray emitting region the problem becomes more acute, and we conclude that it is unlikely that the X-ray emission is due to shocked hot gas.

In addition, the largest allowed change in rotation measure (RM) between the NW hotspot and its surroundings is about 2000rad m^{-2} (Perley & Taylor 1991). At the redshift of 3C295, this converts to an intrinsic $\text{RM} \approx 4000\text{rad m}^{-2}$. A somewhat smaller excess is allowed for the SE hotspot. These values are significantly less than the predicted RMs in Table 2. While multiple field reversals along the line of sight to the hotspots could reduce the predicted values, we note that the observed RMs are fairly constant over spatial scales of 2 kpc, particularly for the NW hotspot. There are thus several problems with a thermal origin for the emission from the NW hotspot.

3.2. Synchrotron Models

Successful synchrotron models have been presented for knot A in the M87 jet (Biretta, Stern, & Harris 1991) and hotspot B in the northern jet of 3C 390.3 (Harris, Leighly, & Leahy 1998). An extension of the power laws from lower frequencies requires that the electron population responsible for the radio (and optical) emission extends to a Lorentz factor $\gamma=10^7$. Extrapolating from the radio/optical spectrum under-predicts the observed X-ray emission by a factor of 500 for the NW hotspot, so a simple synchrotron model is unacceptable. For the SE hotspot, the discrepancy is more than a factor of 1000 (see Figure 3).

Although we have not calculated synchrotron spectra from proton induced cascades (PIC; Mannheim, Krulis, & Biermann 1991), we suspect that such a model would be feasible. The primary difference between the PIC and the SSC models is that PIC involves a very high energy density in relativistic protons

TABLE 3

Synchrotron Input Spectra for SSC Calculation

component	ν_1 (Hz)	ν_b (Hz)	ν_2 (Hz)	α_l	α_h	S_b (cgs)
NW	1E9	1E10	1E15	0.70	1.50	7.08E-24
SE	1E9	1.33E10	1E15	0.70	1.58	3.16E-24

Notes: ν_b is the frequency at which the spectral slope changes and S_b is the flux density at ν_b . The radio spectrum is the peak brightness as observed with a beam size of $0''.2$ (large enough to include the brightest structure seen at 43 GHz, but not so large as to include a lot of surrounding emission). The spectrum is extended to 10^{15} Hz to accommodate the HST data although this has little effect on the derived parameters for the SSC model. The radio spectra are strongly curved (Fig. 3), which cannot be explained either by self-absorption or entirely by spectral aging (given the optical emission). So, following Carilli et al. (1991), we assume that the electron energy spectrum cuts off near the bottom of the observed band. Flux densities are given in $\text{ergs cm}^{-2} \text{s}^{-1} \text{Hz}^{-1}$.

which would indicate a much higher B field (i.e. $> 1000 \mu\text{G}$) than those estimated from the minimum energy conditions assuming the electrons are the major contributor to the particle energy density.

3.3. Synchrotron Self-Compton Model

The radio structure of the hotspots is quite complex, and if we estimate photon energy densities for the brightest regions (from the 43GHz VLA data), we would expect the ACIS detections to be unresolved. Since it is difficult to verify this, we base our calculations on the small volumes, realizing that there may be additional, weaker contributions from somewhat larger scale features (weaker because the photon energy density will be smaller).

Our estimates involve defining the radio spectrum for the brightest and smallest structure of the hotspots (Table 3) and then calculating the synchrotron parameters: the minimum pressure magnetic field, $B_{\min P}$, the luminosity, L_{sync} , and the photon energy density, $u(\nu)$. The spectral coverage of SSC will be determined by $\nu_{\text{out}} \approx \gamma^2 \times \nu_{\text{in}}$, and the ratio of energy losses in the IC and synchrotron channels will be $R = u(\nu)/u(B) \approx L_{\text{ic}} / L_{\text{sync}}$, where $u(B)$ is the energy density in the magnetic field. We can then compute the amplitude of the IC spectrum for which $\alpha(x) = \alpha(\text{radio})$ and which contains the proper luminosity over the defined frequency band.

The calculated SSC values (Table 4) demonstrate that the results are not particularly sensitive to the assumed geometry and that the SSC process is most likely the major contributor to the observed X-ray intensities. In addition to the values shown in Table 4, an SSC estimate for the more extended radio structures of the NW hotspot (i.e. extending $\approx 0''.4$ back towards the nucleus) provides an additional 10% of the total observed flux density at 1 keV.

For magnetic field values of $410 \mu\text{G}$ and $310 \mu\text{G}$ in the NW and SE hotspots (slightly less than the equipartition values in Table 4), the SSC model can account for the entire observed X-ray emission. For even lower magnetic fields, more relativistic electrons would be required, which would result in a greater X-ray luminosity than observed. Hence, these magnetic field values are strict lower limits. The near coincidence of the magnetic field value required by the SSC model and equipartition lends weight to the assumption of equipartition and suggests that the proton energy density is not dominant.

TABLE 4

SSC parameters for the hotspots

geom.	$B_{\min P}$ (μG)	$u(\nu)$ (erg cm^{-3})	R	$S(1\text{keV})$ (cgs)	$S(\text{ssc})/S(\text{obs})$
NW sphere	319	4.4E-10	0.11	2.1E-32	0.57
NW cylin.	561	1.6E-9	0.13	1.9E-32	0.51
SE sphere	271	2.3E-10	0.08	1.3E-32	1.16
SE cylin.	336	2.9E-10	0.06	9.7E-33	0.84

Notes: For the sphere, $r = 0''.1$ (to match the radio beamsize). The cylinder for the NW hotspot has $r = 0''.043$ and $l = 0''.1$. For the SE hotspot, $r = 0''.05$ and $l = 0''.25$. $B_{\min P}$ is the minimum pressure field for no protons and filling factor=1.

4. CONCLUSIONS

The SSC model provides good agreement between the classical equipartition magnetic field estimates and the average field values required to produce the observed X-ray intensities. Since the equipartition estimates were made with no contribution to the particle energy density from protons, this agreement supports the hypothesis that relativistic electrons account for a major part of the the energy density. If future observations show that the X-ray emission is actually extended over a physical distance of 9 kpc, it is unlikely that SSC can be the sole process operating, because the photon energy density will be much lower outside the compact core of the radio hotspot.

SSC is a mandatory process and the only uncertainty in the predictions is the value of the magnetic field. As was the case for the hotspots of Cygnus A, the only viable model to negate these conclusions is one with a much stronger magnetic field: i.e. significantly greater than $500 \mu\text{G}$.

ACKNOWLEDGMENTS

A complex observatory such as Chandra represents a tremendous effort by an extensive team. We thank in particular the ACIS PI, G. Garmire, who was responsible for the detector which allowed us to obtain our results. The work at CfA was partially supported by NASA contracts NAS5-30934 and NAS8-39073. PM gratefully acknowledges support from CNAA bando 4/98. PEJN and TJP gratefully acknowledge the hospitality of the Harvard-Smithsonian Center for Astrophysics.

REFERENCES

- Biretta, J.A., Stern, C.P., & Harris, D.E. 1991, *AJ.*, 101, 1632
- Carilli, C.L., Perley, R.A., Dreher, J.W., & Leahy, J.P. 1991, *ApJ*, 383, 554
- Harris, D.E., Leighly, K.M., & Leahy, J.P. 1998, *ApJ.*, 499, L149
- Harris, D.E., Carilli, C.L., & Perley, R.A. 1994, *Nature*, 367, 713
- Henry, J. P. & Henriksen, M. J. 1986, *ApJ*, 301, 689
- Mannheim, K., Krulis, W.M., & Biermann, P.L. 1991, *A&A*, 251, 723
- Mushotzky, R.F. & Scharf, C.A. 1997, *ApJ.*, 482, L13
- Neumann, D. M. 1999, *ApJ.*, 520, 87
- Perley, R.A. & Taylor, G.B. 1991, *AJ*, 101, 1623
- Taylor, G.B. & Perley, R.A. 1992, *A&A*, 262, 417